Chapter 2

METROLOGICAL CHARACTERIZATION OF RTD FLUXGATE MAGNETOMETERS

Experimental results on RTD-Fluxgate will be presented in this chapter. Experiments, have been carried out on different Fluxgate prototypes; these devices admit of numerous desirable characteristics, including very good resolution, as well as ease of operation, and reduced onboard power requirements.

2.1. PCB FR4 RTD Fluxgate prototype

The starting point of the technological approach presented in this paragraph is a layered architecture of the device, where the ferromagnetic core is just one of these layers.

In particular, the prototype exhibits three layers: two consisting of metalized PCBs FR4 (very similar to that used in standard PCBs but thinner) and a ferromagnetic layer made of Magnetic Alloy 2714A, produced by Metglas ® [2.1]. This choice was guided by the hysteresis characteristic of the material (Fig. 2.1).

In addition, the selected materials selected also exhibit interesting mechanical properties that make the device particularly flexible and durable at the same time, thus widening its scope of employment.
Fifty different prototypes have been realized in order to evaluate the different design solutions (fig.2.3)

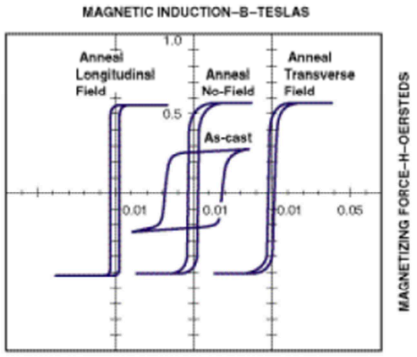

Physical Properties

Density (g/cc)	7.59
Vicker's Hardness (50g load)	960
Tensil Strength (GPa)	1-2
Elastic Modulus (GPa)	100-110
Lamination Factor (%)	>75
Thermal Expansion (ppm/°C)	12.7
Crystallization Temperature (°C)	550
Continuous Service Temp. (°C)	90

Magnetic Properties

Saturation Induction (Tesla)	0.57
Maximum D.C. Permeability (μ):	
Annealed	1,000,000
As Cast	>80,000
Saturation Magnetostriction (ppm)	<<1
Electrical Resistivity (μ--cm)	142
Curie Temperature (°C)	225

Figure 2.1 - BH hysteresis loop, physical and magnetic properties of the Metglas 2714A

Figure 2.2 - Metglas 2714A, sold as a ribbon

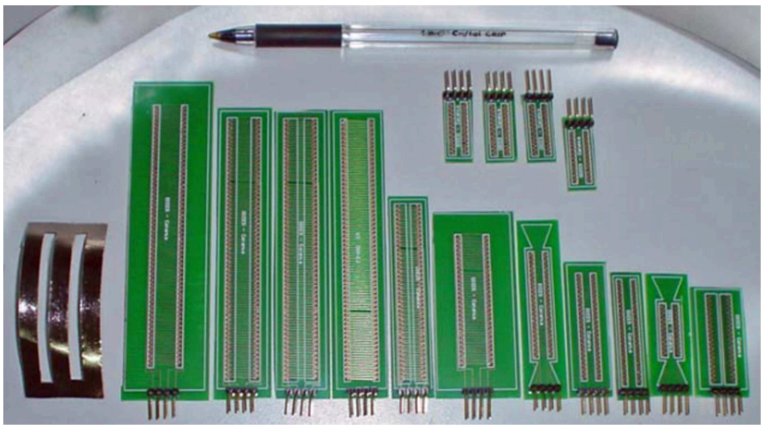

Figure 2.3 - Some of the prototypes of FR4 PCB Fluxgate with embedded Metglas, produced at the DIEES - University of Catania.

The first step of the production process is to obtain a layer of Metglas, patterned according to the desired shape; this layer is then inserted between two PCB-FR4 layers.

After aligning the three layers consistently with the geometry of the sensor, the device is assembled under high pressure at a temperature of 200 ° C. Finally, the vias between the top layer and bottom allows for the realization of the primary and secondary coils (fig.2.5); geometric characteristics of the entire process are shown in Table 2.1. Figure 2.4 shows a schematization of the process just described.

Minimum metal width	200μm
Minimum interspace between metal lines	200μm
Metglas etching mask resolution	100μm

Table 2.1 - Geometrical parameters of the production process with embedded Metglas.

The experimental tests performed on PCB prototypes have shown the applicability of these devices in different situations, such as industrial and of security.
This technology seems to respond to the need to obtain a magnetic field sensor characterized by small size, low-cost and low power consumption, which should offer a resolution in the range of nT.

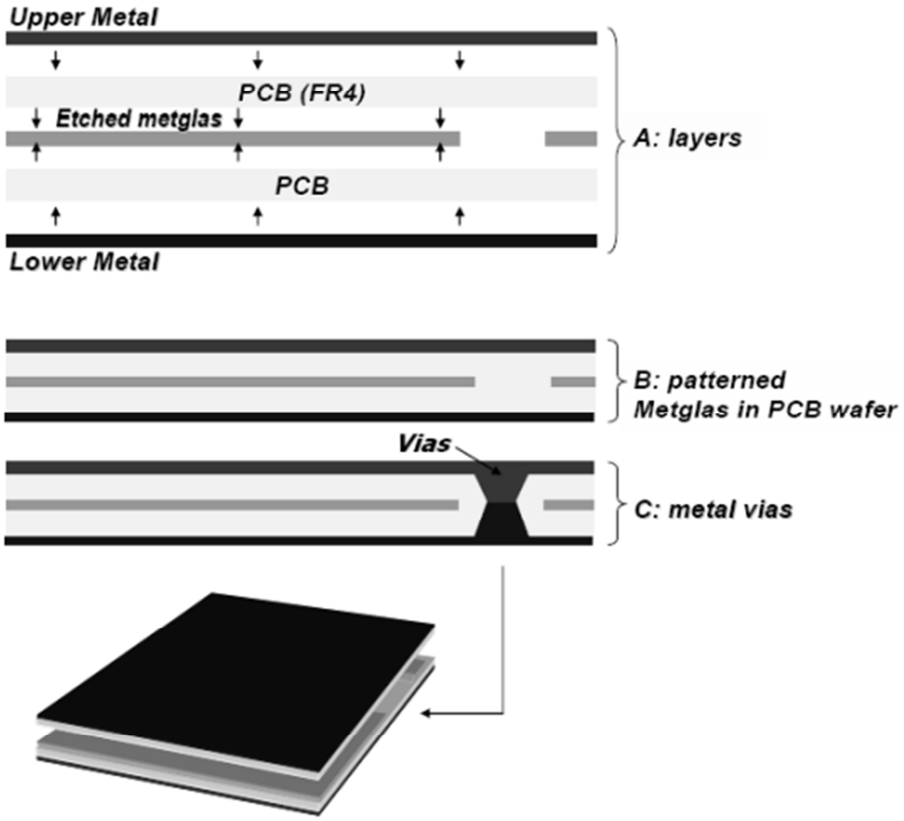

Figure 2.4 - Schematization of the production process

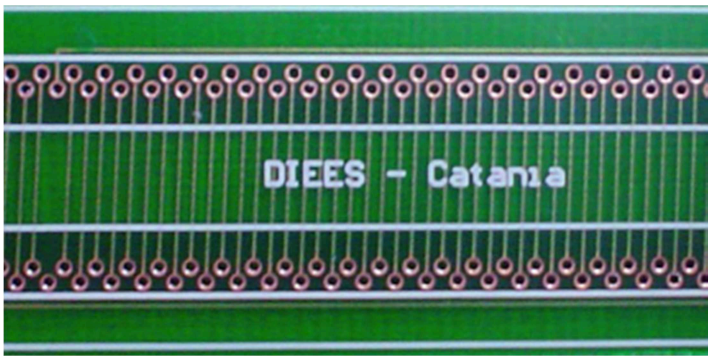

Figure 2.5 - Close view, which allows to notice the vias and the related windings.

2.2. The μWire RTD Fluxgate prototype

The μWire-fluxgate is characterized by a filiform core, with a diameter of about 100 μm, consisting of a ferromagnetic amorphous alloy of FeSiB, obtained by annealing from 80% of Fe, Ni or Co, and 20% of P, Si, Al, C, B [2.2].
The technique used in the production of micro-wire is that of cooling water, with a diameter of approximately 80 to 160 •m and a cylindrical structure.
Typically, the solidification process induces the formation of two different magnetic domains: an inner core, with the easy axis parallel to the wire-axis and an outer coating, with a radial easy axis [2.3] [2.4]. The internal stress induced by the solidification process can be reduced through a process of annealing at 300 - 400 ° C

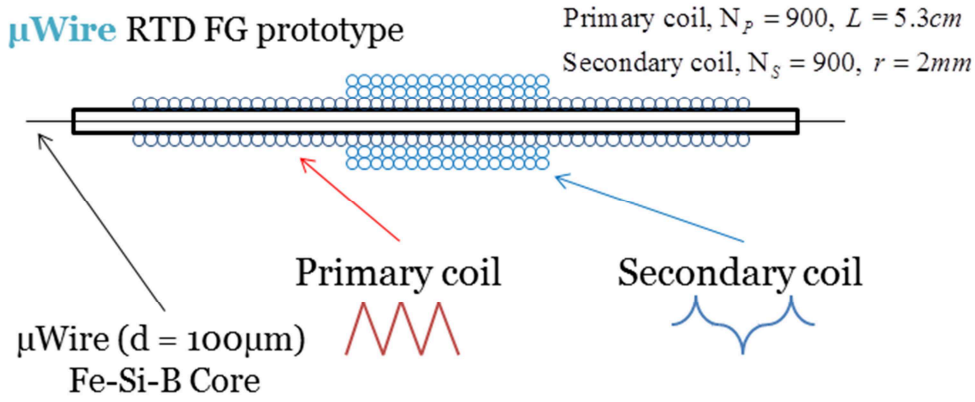

Figure 2.6 – Cross-section schematization of the μWire RTD Fluxgate magnetometer.

The realization steps can be summarized as follows:

- The primary and secondary windings with a wire-diameter of 100 microns are wounded around a plastic structure (whose diameter is about 1.2 mm)
- The micro-wire core is held within an hollow glass cylinder (inner diameter 200 μm, external diameter 2 mm), which acts as a mechanical support.

- The cylindrical support is fixed to the center of the solenoid and the ferromagnetic core is centered on the plastic support.

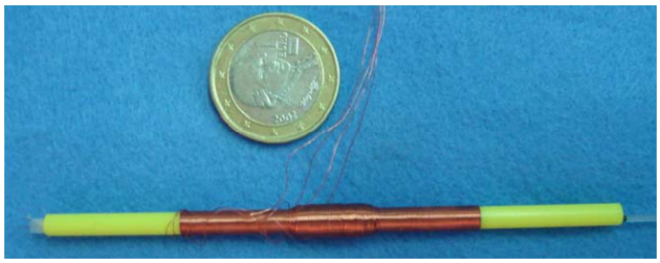

Figure 2.6 – Snapshot of a μWire RTD Fluxgate prototype

Primary coil	**Characteristics**	
	Value	*Units*
Layer number	1	-
Number of turns	~900	-
Coil internal radius	~100	μm
Resistance	30	Ω
Secondary coil	**Characteristics**	
	Value	*units*
Layer number	4	-
Number of turns	~900	-
Coil internal radius	~100	μm
Resistance	30	Ω

Table 2.2 - Mechanical and electrical parameters of the μWire RTD Fluxgate

The μWire Fluxgate has interesting physical properties and an high spatial resolution. The mechanical flexibility of the structure can be exploited, for example, in those measurement situations where the core is bent to form a closed magnetic path for the detection of magnetic particles [2.4]

The spatial resolution of a fluxgate magnetometer is strictly related to size of the ferromagnetic core. This suggests the use of this particular prototype in all that applications where the sensing of small, spatially distributed magnetic sources is needed, which happens in most of biosensors applications such as magnetic immunoassay, gene segmentation, spot detection, etc.

2.3. Definition of operating conditions and metrological characteristics

It is crucial, especially for practical purposes, the definition of a standard procedure for the characterization of this type of magnetometer. In this section, some considerations about the estimation of sensor performance, are given. These considerations are valid regardless of the realization technology.
The characterization of a device, should start from an accurate analysis of the main parameters that define the operating condition. In the case of Fluxgate magnetometers, these parameters are:

- observation time, T_{OBS}
- forcing signal amplitude, A
- forcing signal frequency, f
- target magnetic field intensity, H_X

The purpose of this study was to quantify the performance of the sensor versus the variation of the four parameters. The results of this analysis, then led to description of a possible algorithm for the choice of values to be assigned to such parameters that will be explained later.

The observation time, T_{OBS}, is the temporal dimension of the window on which the output signal is averaged. The more we are willing to wait, the better is the precision on the measurement.
The observation time is a parameter whose value could be given by the

problem itself (as in critical applications, where information of the sensors must occur at a precise rate defined a priori) or may be derived from a certain desired performance.
The amplitude and frequency of the driving signal (*A* and *f*) are the two parameters that affect more the trade-offs between performance and power consumption. As previously mentioned, the fluxgate is excited with a periodic current, in order to produce an excitation magnetic field He, whose amplitude must satisfy the relation: $|H_X| < \widehat{H}_E - H_C$
If H_E is not high enough to overcome the coercive field threshold, H_C, the device does not switch over from one state to the other and, consequently, the output voltage would be missing one of two peaks (or both if H_X = 0). This is summarized graphically in Figure 2.7

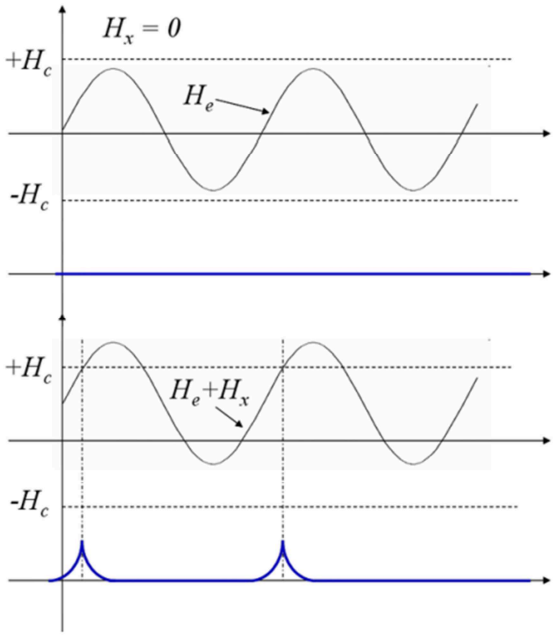

Figure 2.7 - Operation out-of-range sensor. The blue curve represents the voltage output of the device.

For what concerns the driving frequency, the lower limit is dictated by the need to obtain a good magnetic coupling between windings. At very

low frequencies (e.g., below 40 Hz) the device begins to show a rather noisy output, in addition, with decreasing frequency, decreases obviously also the rate of *RTD* values in a given time interval. In fact, by adopting a time readout technique, we obtain a *RTD* value for each period of the magnetic field bias. Consequently, fixing a-priori the number of samples to be acquired (n), the observation time, is a function of the driving frequency, according to the relation: $T_{OBS} = n/f$.

It has to be borne in mind that the sensitivity is inversely proportional to both the amplitude and the frequency of the driving signal (see chapter 1), so it's not always convenient to work with a strong excitation current. From this consideration arises the most important trade-off for this kind of device; the operating condition should be tuned in each case, depending from the application (Table 2.3).

	Operating range	Linearity	Band-width	Noise	Sensitivity	Power
Higher excitation frequency	Not affected	Not affected	wider	lower	lower	Sligthly higher (mainly for the digital domain)
Higher excitation amplitude	larger	better	Not affected	lower	lower	higher

Table 2.3 – Influence of the driving amplitude and frequency on the main metrological parameters of the magnetometer

The external magnetic field Hx, is the last important parameter to consider. As mentioned in chapter 1, a DC target, parallel to the sensor, corresponds to an offset applied to the bias field and determines the residence times in the two stable states; in order to work within the allowed operating range, the relation $|H_x| < \widehat{H}_e - H_c$ must be always satisfied. To give an idea, with typical values for (H c, He) = (1.6 A/m, 6.8

A/m), the constraint on terms of the external field is reduced to: |Hx| < 5.2 A/m = 6.5•T.

From a practical point of view, the sensor is subjected, in addition to the effect of target also to a component due to the presence of noisy sources the measure environment. Assuming that this component is constant in the measuring time interval and does not exceed the operating range, the consequences are, in most cases, minimum. In fact, if the interest is only in a relative measure (which is quite common for this type of sensors) as long as H_X remains within the operating range, the behavior of the device remains virtually unchanged in terms of input-output relationship (thanks to the high linearity of the magnetometer).

This partially redefines the meaning of the parameter H_X as the sum of the magnetic noise in the environment and the value of the target to be measured.

After having analyzed the parameters that define the operating condition, now we see how the sensor performance changes in terms of these parameters.
In particular, we focus on the three following metrological characteristics:

- Sensitivity, S [μs/nT]
- Resolution in terms of time, •s [μs]
- Resolution in terms of magnetic field, •T [nT]

Typically happens that, in each application, these parameters assume a different importance. It is hence essential to know how to act on user-controllable parameters (T_{OBS}, A, f) to get from the device the desired behavior.

2.3.1. Sensitivity

We define sensitivity, S, as the ratio between the change in output the device and the corresponding change in the input that caused it:

$$S = \frac{\Delta OUT}{\Delta IN} = \frac{\Delta RTD}{\Delta H_X}$$

In our case, the input is represented by the external field H_x, and the output is the RTD value calculated starting from the sensor output.

With reference to Figure 2.8, in the case of sinusoidal forcing, in the areas highlighted in pink a small perturbation of H_x produces a large change in RTD. So these are areas of maximum sensitivity, near the limits of the operating range, where, at least theoretically, one should work. In the practice however. this could be done only by introducing a closed loop control on the offset of the driving signal, in order to satisfy, the constraint that defines the operating range. In any case, this strategy reveals to be rather complex and poorly successful, as evidenced by the numerous tests experiments conducted in this regard.

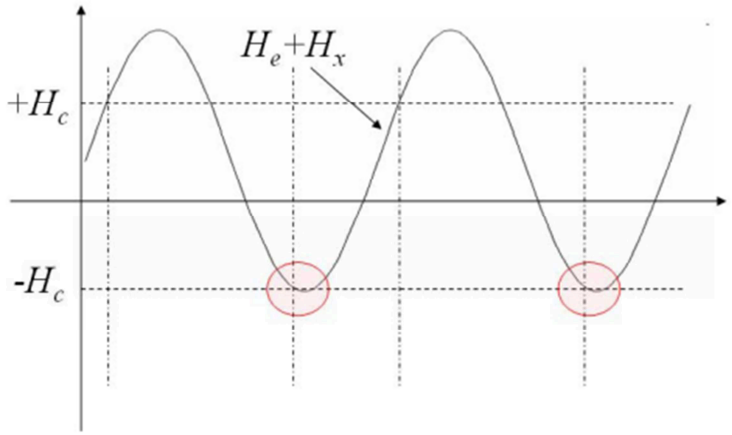

Figure 2.8 – Maximum sensitivity condition.

2.3.2. Resolution

Adopting, as mentioned, a time-domain readout strategy, the sensor output will be obviously a time. We define the resolution as the slightest change in the value of the measurand, ΔH_X' around a value of H_X, which leads to a change in the output $\bullet RTD'$ whose amplitude is equal to the uncertainty of measurement $\bullet RTD$:

$$\frac{dH_X}{H_X} = \frac{\Delta RTD}{\Delta RTD'} \frac{\Delta H'_X}{H_X}$$

From a practical standpoint, since the distribution of values of the RTD is typically gaussian, the resolution value, given the observation time, coincides with the standard deviation of the distribution of the mean values divided by the sensitivity of the device:

$$Resolution(T) = \frac{std[\overline{RTD}(T)]}{sensitivity}$$

Where T is the observation time and the operator "std" is the standard deviation. This is typically the reference parameter of quality in the magnetometry field, as it is dimensionally consistent with the measurand.

2.4. Testing and calibration Set-up

There exists two methods for the calibration of the sensor sensitivity. The first one uses the Earth's field, the second needs calibration coil. Practical reasons exclude the use of the earth's field, that requires precise globe positioning of the sensor under test. This calibration procedure is well described in geophysical literature [2.5]. For the measurement of sensor noise, environment with very low magnetic field is required. Shielding of the ambient field is usually performed by ferromagnetic shielding made in the form of a multilayer cylinder from Permalloy or amorphous materials [2.6]. The calibration instruments adopted in this work consists of the cylindrical

solenoid presented in Figure 2.9a and from the three layers Metglas magnetic shield showed in Figure 2.9b.

It is worth to affirm that solenoids are not very practical calibration instruments because access to their centre, where the sensor under test should be located, is complicated. The most common calibration tool is the Helmholtz coil pair, shown in
Figure 2.10, which consist of two identical, thin, circular coils separated by a distance of their radius.

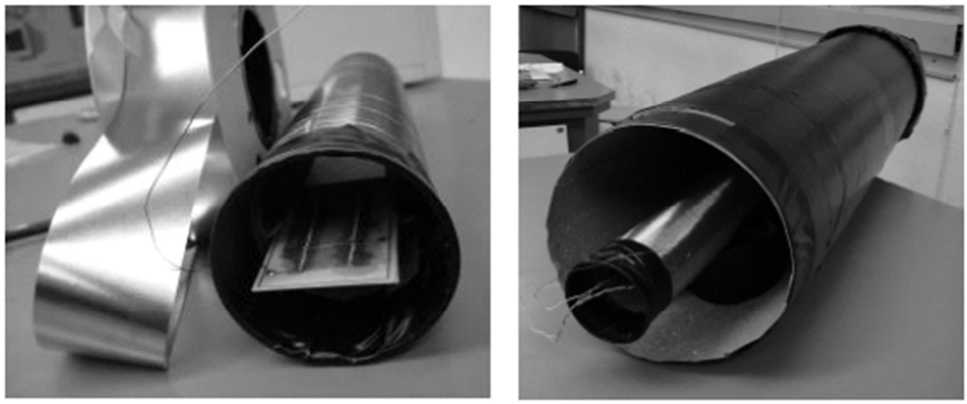

Figure 2.9a - Solenoid used to generate the target signal; Figure 2.9b Dc magnetic shield.

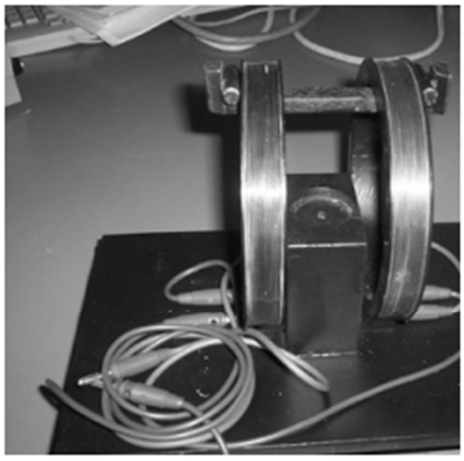

Figure 2.10 - Helmholtz coil.

The solenoid and the sensor operate inside the shield for dc magnetic field. In order to define a priori the shielding characteristic we made the following considerations; defining:

$$G = \frac{H_{external\ to\ the\ shield}}{H_{inside\ the\ shield}}$$

the ratio between the environment field and the field inside the shield, the efficiency • of the ferromagnetic multi-layer adopted, is determined by:

$$\eta\% = 100\left(1 - \frac{1}{G^n}\right)$$

where n is the number of layers adopted in the shield design. For a cylindrical shield [2.7], the approximation:

$$G \approx \frac{\mu_r t}{2b}$$

may be used, where $\bullet_r$ is the magnetic permeability of the shielding material, t is its thickness, and b the external radius of the cylinder. Considering the high permeability of Magnetic Alloy 2714A and keeping b low (as constrained by the dimensions of the coil), a shielding efficiency of 98% was obtained with only three layers.

2.4.1. The electronic circuit for the operation of RTD Fluxgate magnetometers

The purpose of electronics for signal conditioning is to provide an electrical signal, typically a voltage, easily processable, from which it is possible to extract useful information (in our case, as mentioned, the value

of *RTD*). Will now be displayed in a schematic way, the design process of the electronic circuits used for the operation of the magnetometer. For this purpose it is convenient to start from a black box representation of the Single Core Fluxgate Magnetometer (Fig.2.11)

Figure 2.11 – Black-box representation of the SCFM

Where Iexc is the periodic excitation current, V_{OUT} is the output voltage at the secondary coil. The goal of electronics is twofold: to supply I_{EXC} and to properly process V_{OUT}.

2.4.1..1 The excitation stage

With regard to the excitation current, it is necessary to design an analog block able to provide an AC current. Specifications are 100mApk regarding the amplitude, bandwidth from DC to 1 kHz, low harmonic distortion and low noise. The implementation of this first block analogue was made as shown in the following figure:

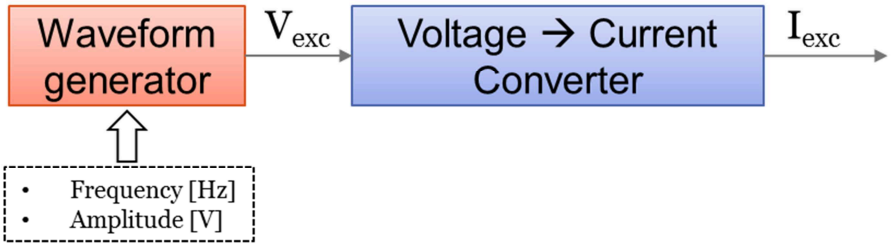

Figure 2.12 – The excitation stage

A waveform generator provides a periodic voltage (sinusoidal, triangular, etc.) of arbitrary amplitude and frequency. This block is achievable in the practice in many different ways, for example:

- Function Generator (useful for the metrological characterization because it provides maximum performances in terms of noise and harmonic distortion and high flexibility because it can be remotely controlled by GPIB, RS-232 or USB)
- Analog Integrated Circuit for waveform generation (there are several available on the market although they have been almost completely replaced by digital alternatives)
- Microcontroller + DAC + Low Pass Filter (this is the preferred solution if the goal is to make a PCB for autonomous operation of the sensor)

The voltage supplied by the function generator must be properly scaled and then converted into a current. A standard approach is to realize a op-amp voltage-current converter with floating load (as none of the two terminals of the primary winding should be shorted to ground). In this topology, the resistance R_T performs the transduction simply according to Ohm's law $I_{EXC} = V_{IN} / R_T$. The operational acts primarily as a buffer, providing the required current to the load without affecting the input signal.
To increase the flexibility of this solution, the fixed resistor R_T can be replaced with a digital potentiometer (e.g. MCP41xxx and the like) so it is possible to change the amplitude of the excitation current through serial communication SPI4/I2C.

2.4.1..2 The amplification stage

The differential output voltage, taken across the secondary winding, has typically very low dynamic (<10mVpp) and the common mode noise is quite high. This suggests the use of an instrumentation amplifier in order to obtain the following three key-benefits:

- differential to single-ended conversion
- High CMRR
- Linear Amplification with gain settable by a single resistor

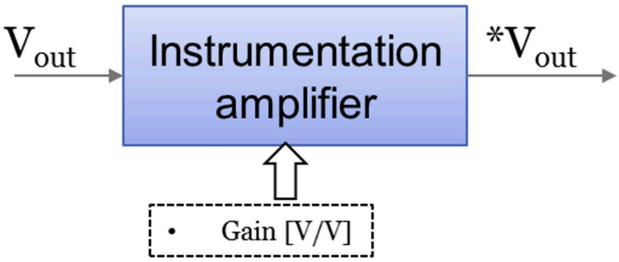

Figure 2.13 – The amplification stage

Again, it is convenient to replace the gain resistor with a digital potentiometer, in order to greatly increase the flexibility and applicability of the circuit.

2.4.1..3 The Schmitt Trigger stage

One of the biggest advantages of a time-domain readout strategy is obviously to be able to operate in the digital domain for reading the output signal, which, in the case of the *RTD* fluxgate, is a difference between time intervals. It is therefore necessary to process the amplified output voltage of the sensor in order to obtain a signal that can drive properly a set of digital timers. For this purpose, a comparator with hysteresis (Schmitt trigger) has been implemented.
In this way we obtain a square wave whose duty cycle is a function of the *RTD* according to the relation: *RTD = T [2d-1]* where *T* is the period of the excitation current and the duty cycle expressed as *T+ / T*.

It is worth mentioning the presence of a level shifter between the instrumentation amplifier and Schmitt trigger as the dynamics of the comparator input is TTL (0-5V) and not bipolar voltage as the output voltage of the magnetometer.

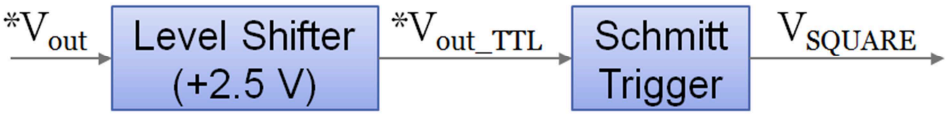

Figure 2.14 – The Schmitt Trigger stage

2.4.1..4 The readout and communication stage

Starting from the square waveform supplied by the comparator, a measurement of time intervals using digital counters is performed. In this way we obtain a measure of *RTD* for each period of the excitation current. This data can be used by an onboard microcontroller (for example to turn on a light or to be displayed on a display) or it can be transmitted to a sink node both in wired mode (RS232, USB, SPI, I2C, etc.) or wireless (ZigBee). The presence of a microcontroller allows a preprocessing the data before the actual transfer of the same to the sink node.

Figure 2.15 – The readout and communication stage

The clock frequency of digital timers is a critical parameter that determines the resolution. The design of the digital sub-circuit is therefore crucial in order to maximize the resolution of the overall system.

2.4.2. The electronic circuit for the Single Core Fluxgate Magnetometer

After having outlined schematically the main stages that constitute the driving, conditioning, and readout circuit, it is possible to discuss its actual realization.

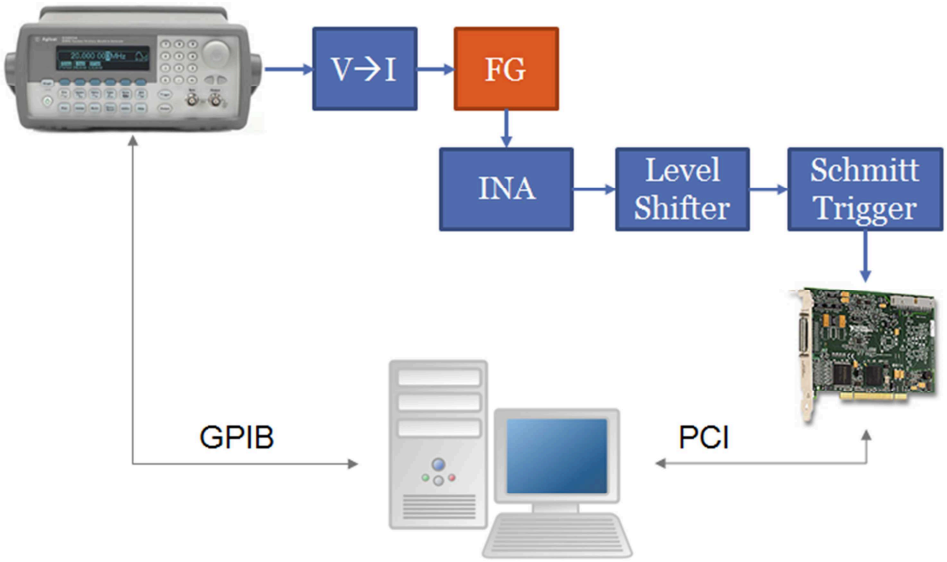

Figure 2.16 – Overview of the electronic circuit and the equipment involved in the metrological characterization of the Single Core Fluxgate Magetometer

In this case, the target the realization of a performing and flexible circuit, easily connectable to external equipment and pre-existing characterization setups.

The wave generator is represented here by a traditional periodic function generator, remotely controlled via GPIB communication. The output of the Schmitt trigger drives directly the counters of a digital acquisition board from National Instruments PCI (PCI-6221) which offers two 32-bit counters @ 80 MHz. The data is then processed by the measurement software that runs on the PC (developed within the LabVIEW environment), in addition the acquisition software manages all the operations of streaming data to disk for later analysis.

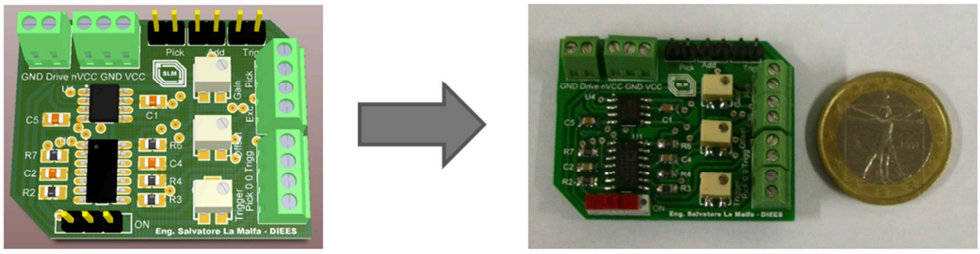

Figure 2.17 – 3D representation of the electronic circuit (left), snapshot of the actual PCB (right)

This circuit was implemented on an FR4 PCB with four layers and has been effectively used for the metrological characterization of SCFM.

2.4.3. The electronic circuit for the Coupled Core Fluxgate Magnetometer

A rather simplified schematization of the circuit for the CCFM (three nodes) is presented in figure 2.18:

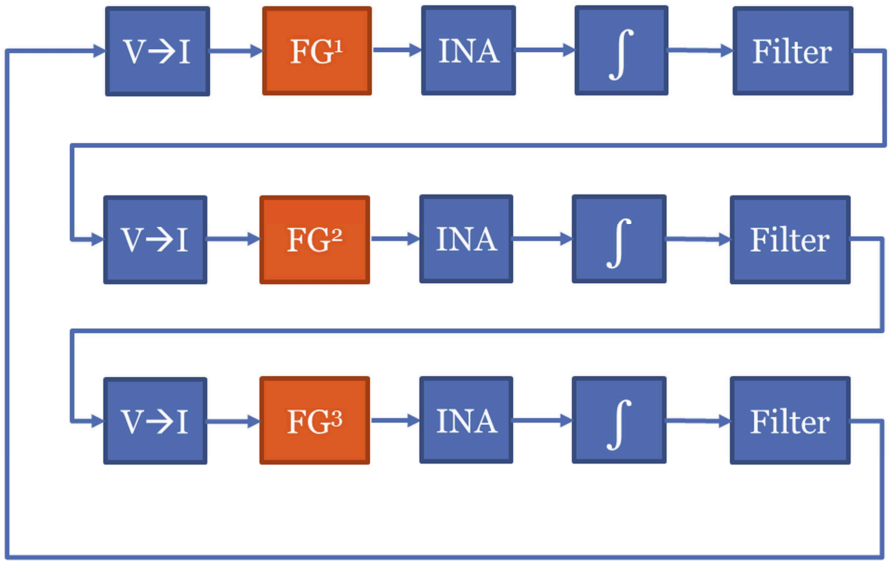

Figure 2.18 – Simplified Block-diagram schematization of the electronic circuit for the CCFM operation

As can be seen from this schematization, the coupling signal is represented by the integral of the output voltage. This signal is therefore proportional to the magnetic flux that has a nearly square waveform. In this case it is therefore convenient to work on this signal directly, without having to use to the Schmitt trigger as in SCFM case. The use of a TTL zero-comparator without hysteresis it's enough in order to obtain a signal compatible with digital timers, both in terms of voltage levels and steepness of the edges.

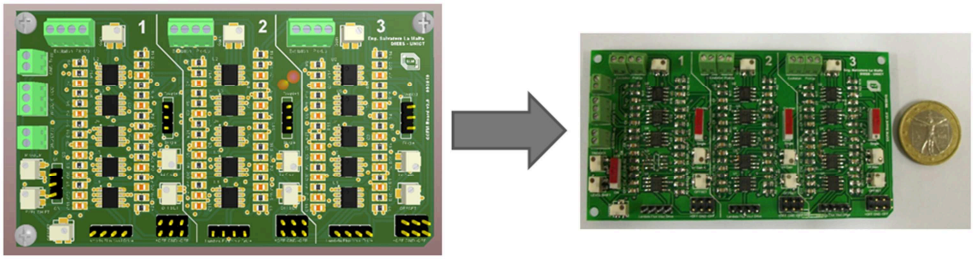

Figure 2.19 – 3D representation of the electronic circuit (left), snapshot of the actual PCB (right)

2.5. Experimental Results

In this section experimental results about the metrological characterization will be briefly reported, highlighting the experimental procedure behind the measurement process.

What follows is not intended to represent a complete characterization report of the device (since it has been already done elsewhere). It is instead a presentation of some of the interesting results obtained during my Ph.D activity.

2.5.1. Perming effect

The perming effect can affect the output signal of the device (by an offset) after a magnetic shock. It is similar to hysteresis, but the applied field must be much higher than the full-scale range. All the sensors containing ferromagnetic material are susceptible to perming. This procedure ensures a defined magnetic state and is called re-magnetization. In the case of fluxgate sensors, the re-magnetization is performed by forcing a current through the primary coil. Anyway, it must be considered that no significant perming is observed if the device is polarized by a high current value [2.8].
To suppress the offset, it might be useful to employ the same technique used by the AMR sensor [2.9], consisting in the application of a high current pulse to the core to stabilize its the magnetic status before the normal operation of the sensor.

2.5.1..1 The experimental set – up to investigate the perming offset

The experimental set-up consists of a Residence Times Difference fluxgate magnetometer (μWire prototype) operated with a triangular bias current @ 80 Hz and a 4-layers solenoid in order to produce the external reference target magnetic field necessary for the sensor characterization. The experimental characterization procedure is schematized in Fig.2.19 and consists of six consecutive steps:

A. In the first step the amplitude of the driving current is linearly decreased to zero.
B. A triangular shaped magnetic field is forced through the external solenoid to infer the core re-magnetization. The amplitude of the applied field must be high enough to ensure a sufficient saturation of the core (in our case the peak-to-peak amplitude is 20mT). During this phase the magnetometer is not driven by any excitation current as it could vary its magnetic state.
C. The driving current is restored to its nominal value.
D. 30 seconds of the output signal (*RTD*) with nominal zero applied field are acquired.
E. A high DC magnetic field is applied through the external solenoid for 15 seconds.
F. The applied field is turned off and a *RTD* shot of 30 seconds is acquired. As it can observed an offset appears in the output signal as respect to the same signal analyzed in phase (D). This quantity, divided by the sensor sensitivity, can be considered as the perming offset. It must be noted that the output signal of the sensor is not acquired during phases A, B, C and E (grayed areas in Fig.2.19).

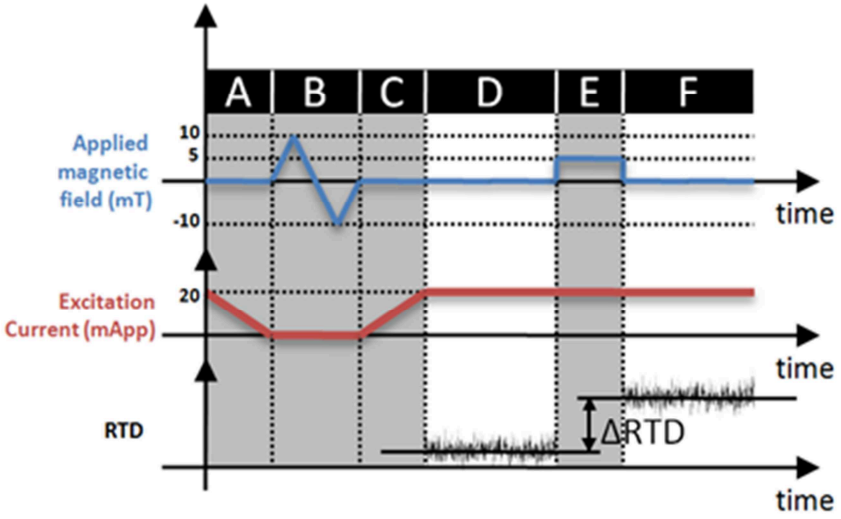

Figure 2.20. Qualitative schematization of the experimental procedure

Experimental results concerning the estimation of the perming offset in the μWire RTD fluxgate are summarized in Fig. 2.20. For each excitation current amplitude [2, 5, 10, 15 20] mApp the variation of the *RTD* measured before and after the application of the magnetic shock, •*RTD*, was estimated. Results obtained show that the perming effect increases quite linearly with the field intensity. Moreover, this effect is less evident when excitation current amplitude increases. This is quite reasonable because an higher driving current produces a higher saturation of the ferromagnetic core that hence becomes less susceptible to perming.

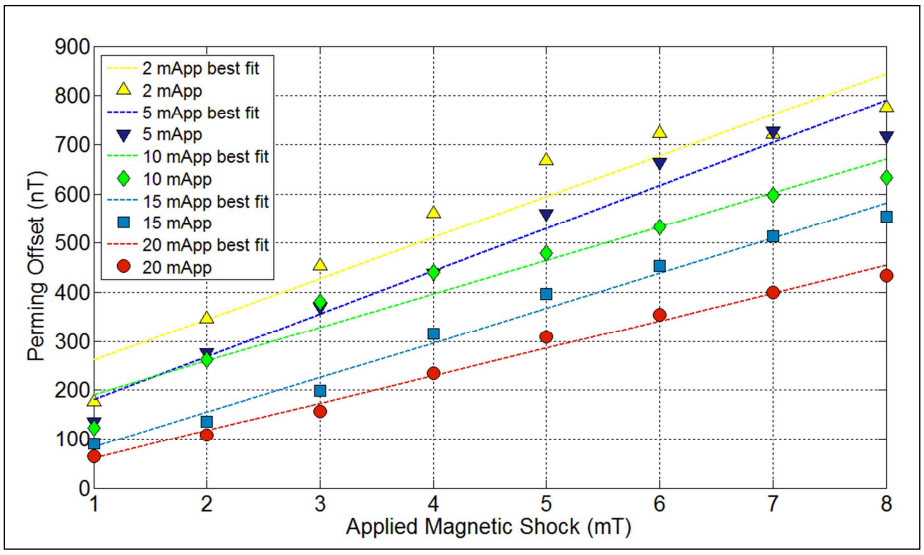

Figure 2.20. Experimental results on Perming estimation. The reported perming offset is calculated as the delta-RTD consequent to the magnetic shock divided by sensor's sensitivity.

The obtained experimental results show the possibility to implement an optimal re-magnetization strategy of the ferromagnetic core for the particular case of RTD fluxgate magnetometers.

2.5.2. Resolution measurements: SCFM vs CCFM

A comparative metrological characterization of the two RTD Fluxgate systems has been carried out in order to obtain a quantitative estimation of the device's performances in real world applications.
The measurements were carried out inside an anechoic chamber in order to have an extremely controlled environment by the electromagnetic point of view. The characterization setup is shown below:

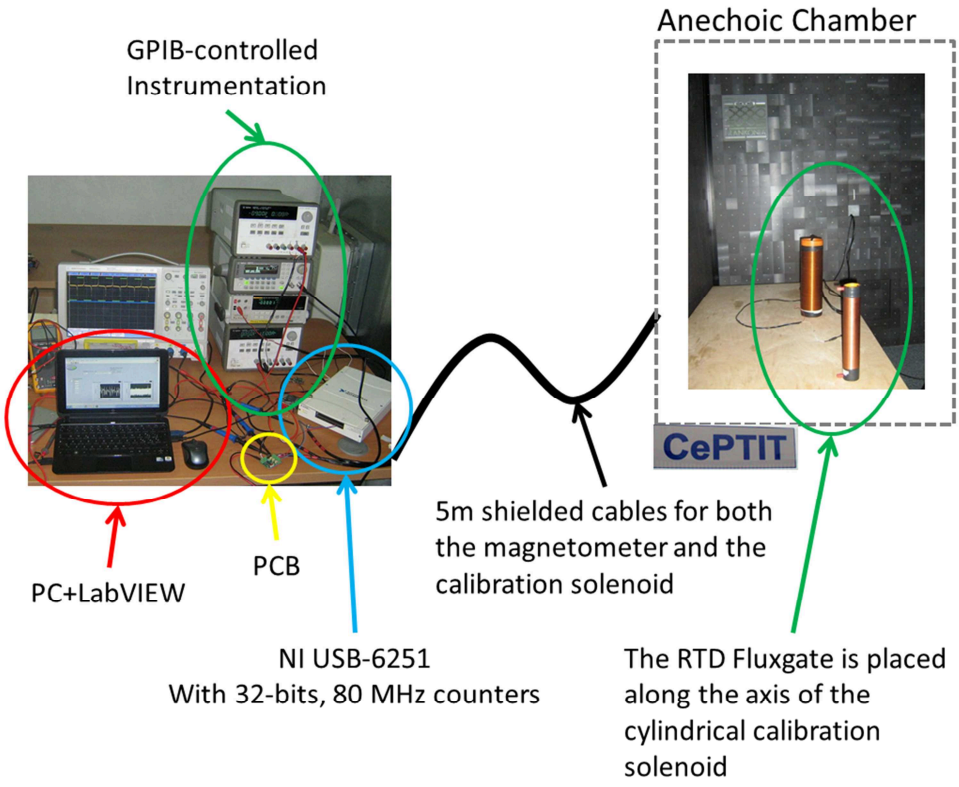

Figure 2.21. Overview of the characterization experimental setup

In order to minimize the uncertainty associated with the open-loop applied magnetic field intensity a FEM analysis was performed (Fig. 2.22)

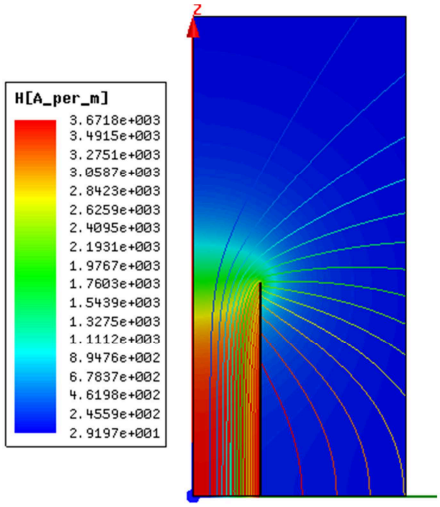

Figure 2.22. FEM analysis on a cylindrical calibration solenoid. The results of this analysis have been exploited in order to minimize the uncertainty on the magnetic field intensities applied during the calibration process.

The characterization procedure can be summarized as follows:
First of all the operating condition must be chosen. In the case of the SCFM this means, as seen so far, the amplitude and the frequency of the driving signal. With regard to the CCFM, since there is no driving signal in this case, the operating condition is determined by value of the coupling strength parameter, λ. This value also fixes the oscillation frequency of the three devices coupled in the ring.

The first data acquisition is made with zero-applied field in order to observe the temporal evolution of the *RTD* within a quite long time window (usually > 30 s). This data contains the information about noise and its thus crucial from the estimation of the resolution (fig.2.23).

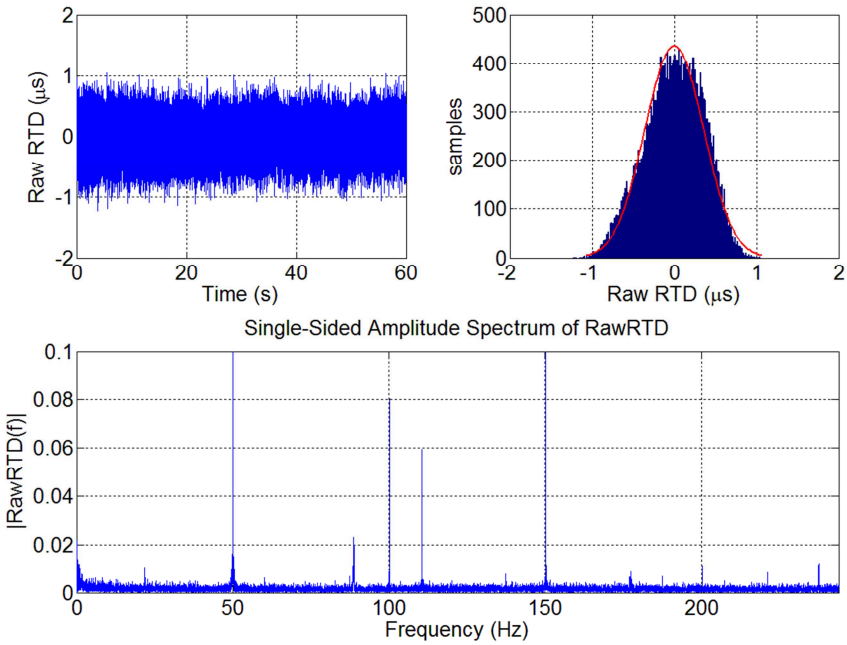

Figure 2.23. (top-left) temporal evolution of the unprocessed *RTD* samples versus the observation time. (top-right) histogram of the raw *RTD* data. Notice the Gaussian distribution, starting hypothesis for the successive elaborations. (bottom) FFT of the raw RTD. The tones of higher amplitudes (at 50Hz, 100Hz 150Hz and aliases as well) are due to the noise coming from the power supply.

then a DC target magnetic field of varying intensity is applied in order to estimate the sensitivity of the device. In this way the so-called "calibration curve" is obtained (fig 2.24). Starting from the raw RTD @ zero field and the sensitivity value of the magnetometer is finally possible to calculate the resolution of the magnetometer versus the observation time. This parameter is defined as follows:

$$Resolution(T) = \frac{std[\overline{rawRTD}(T)]}{sensitivity}$$

Where the rawRTD(T) is the distribution of the averages of the rawRTD within a time-window of T.

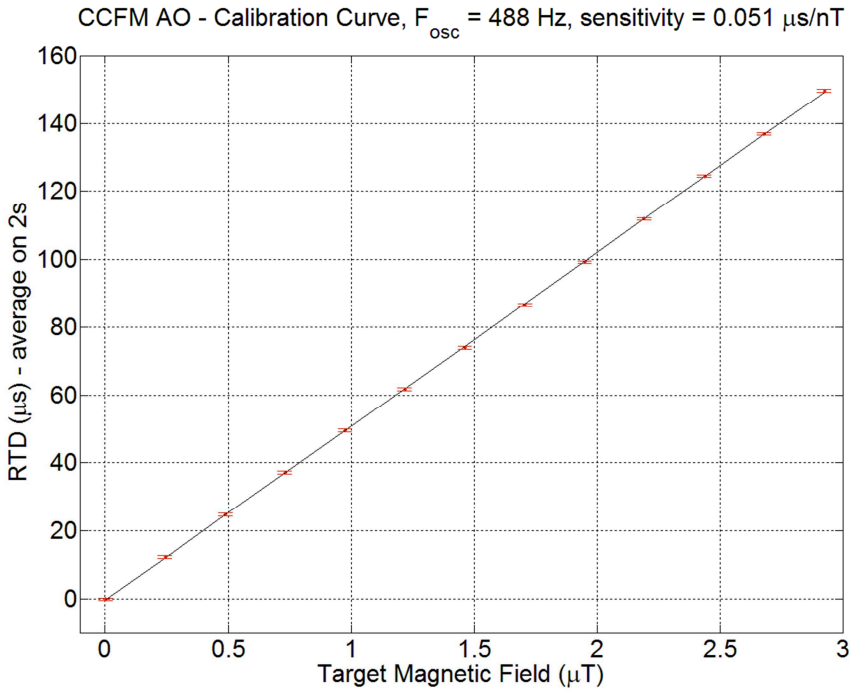

Figure 2.24. Calibration curve of the Coupled Core Fluxgate Magnetometer. The slope of this curve is the sensitivity of the device.

Then a comparison between the resolution of the CCFM and the SCFM is shown in fig. 2.25. The CCFM exhibits a better resolution, even for short observation times. This confirms the expectations because for the same noise floor, the coupled system offers greater sensitivity. However, from a practical point of view, it should keep borne in mind that the CCFM is a significantly more complex device than the SCFM, both as regards the structure, certainly more cumbersome and brittle, both in terms of the circuitry that definitely needs more power. Having said that, in all those applications where it is needed a pushed resolution even at short observation times, the CCFM is the best solution. In all other situations it is advisable to use the SCFM instead, mainly because of its simplicity and its smaller size.

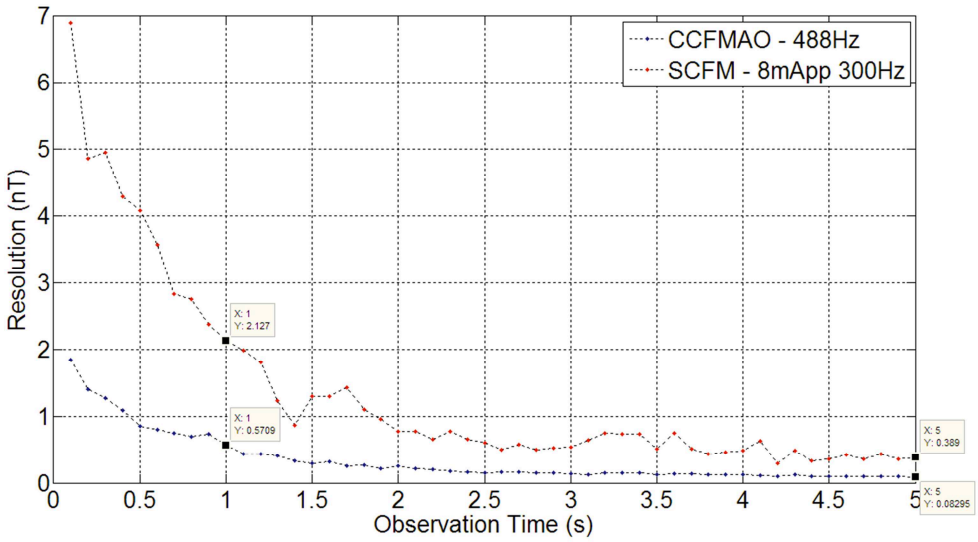

Figure 2.25. Resolution versus observation time. The CCFM exhibits a better resolution thanks to its greater sensitivity.

References

[2.1] P. Ripka: Magnetic Sensors and Magnetometers. Artech House, Boston,(2001).
[2.2] www.metglas.com
[2.3] H. Chiriac, J. Yamasaki, T. A. Ovari, M. Takajo, Magnetic domain structure
in amorphous glass-covered wires with positive magnetostriction, Magnetics, IEEE
Transactions on, Vol.3, issue 5, pp. 3901-3903, 1999.
[2.4] H. Chiriac, Internal stress distribution in glass-covered amorphous magnetic
wires. Physical Review, vol. 52, n. 14, October 1995.
[2.5] J. JanKowsky, C. Sucksdorff: Guide for magnetic measurements and Observatory Practice. Warsaw, Poland: IAGA, (1996).
[2.6] P. Ripka: Advanced in Fluxgate sensors. Sensors and Actuators A, vol. 106, issue 1 3, pp. 8-14 (2003).
[2.7] E. Durand; MAGNÉTOSTATIQUE. Masson et Cie, Editeurs, PARIS-VI (1968)
[2.8] P. Ripka, Magnetic Sensors and Magnetometers. Boston, MA: Artech House, 2001.
[2.9] Honeywell, “1- and 2-Axis Magnetic Sensors, HMC 1001/1002 and HMC1021/1022,” Datasheet 900248 Rev. B.